Electronic Supplementary Information (ESI)

Light-promoted C−Cl bond-forming reductive elimination of a metal-metal bonded Pd^{III}–Pd^{III} complex

Jeongcheol Shin, Kuldeep Gogoi, and Kiyoung Park*

Department of Chemistry, Korea Advanced Institute of Science and Technology (KAIST), Daejeon 34141, Republic of Korea
*Correspondence to: kiyoung.park@kaist.ac.kr

Table of Contents

Methods and Materials

Material Synthesis. Reagents were purchased from commercial suppliers (Alfa Aesar, Sigma-Aldrich, and Acros Organics), stored under N_2 conditions, and used as it is. All reactions were performed under anaerobic and dry conditions by using N_2-filled glove boxes and Schlenk lines, as following previously reported synthetic protocols for $PhICl_2$ in ref [1], $[(phpy)Pd^{II}(OAc)]_2$ in ref [2]. $[(phpy)Pd^{III}(OAc)Cl]_2$ (**1**) and 2-(2-chlorophenyl)pyridine (**2**) were synthesized with the same protocol as $[(benzo[h]quinoline; bzh)Pd^{III}(OAc)Cl]_2$ but performed at a lower temperature of $-35\ °C$.[2]

Spectroscopic details. *Nuclear Magnetic Resonance (NMR) spectroscopy.* The formation and purity of synthesized compounds were confirmed by ^1H-NMR spectra collected on a Bruker 400 MHz Avance III NMR spectrometer equipped with a BBFO probe. All NMR samples were anaerobically prepared in airtight J-Young NMR tubes using acetonitrile-d_3 solvent.

Electronic absorption (Abs) and magnetic circular dichroism (MCD) spectroscopies. A JASCO J-1500 CD spectrometer was used for both Abs and MCD spectra. The temperature of samples was controlled by using a Unisoku cryostat. The MCD spectra were collected in the solenoid core bore of a Cryomagnetics 5T cryogen-free superconducting magnet.

Resonance Raman (rR) Spectroscopy. The rR spectra collected with visible laser lines were measured on an Andor SR-750-A-R spectrometer equipped with 1200 and 1800 l/mm gratings, an Andor iVac DR-316B-LDCDD-RES detector, and Changchun New Industries optoelectronics 532, 515, and 488 nm lasers. Spectra obtained with NIR excitations were collected with an Andor SR-303i spectrometer equipped with a 1200 l/mm grating, an Andor iVac DR-324B-FI-RES detector, and an Innovative Photonic Solutions 785 and 633 nm laser. The powder sample of **1** was prepared in 4 mm EPR tubes and kept in a $N_2(l)$-containing finger dewar during the data collection. The powder sample of $[(phpy)Pd^{II}(OAc)]_2$ was prepared in capillary and measured at 298 K.

Electron Paramagnetic Resonance (EPR) Spectroscopy. The EPR spectra were collected with a Bruker EMXplus X-band EPR spectrometer equipped with an ER4141VT variable temperature controller and an ER4119HS cavity liquid nitrogen cryostat. Samples were frozen and stored under liquid nitrogen before measurement. EPR data were collected at 100 K.
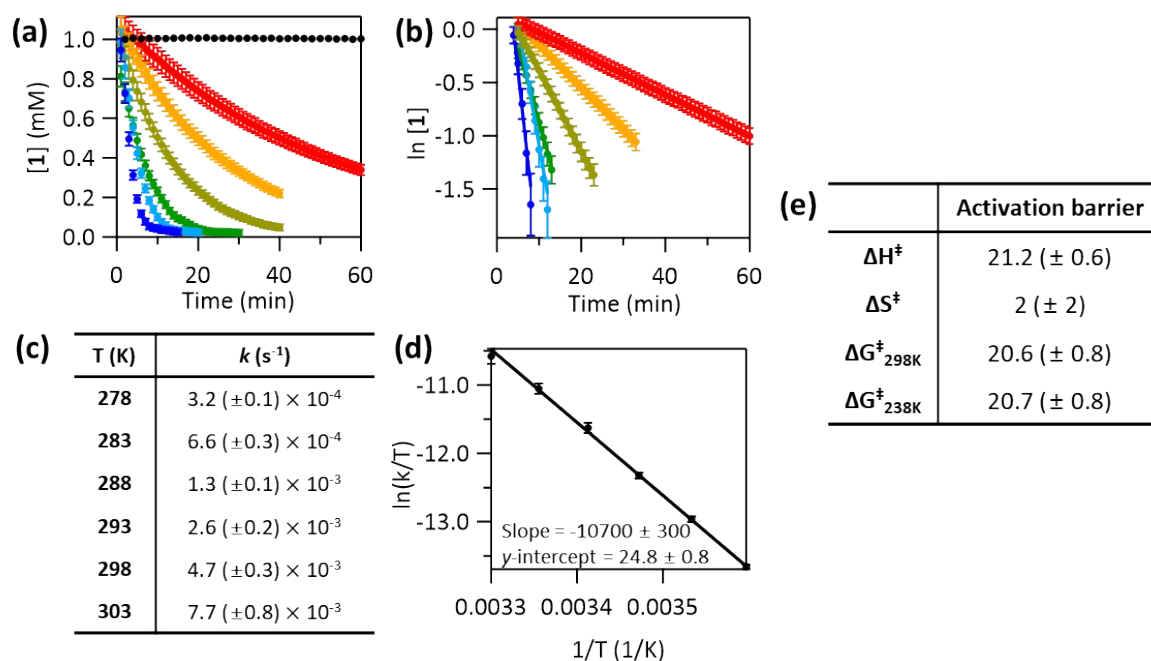
Photo-induced reactions. $[(phpy)Pd^{III}(OAc)Cl]_2$ (**1**) was dissolved in acetonitrile at $-35\ °C$, and 330 μL of the solution was transferred to an airtight cuvette that was precooled to $-35\ °C$ in the N_2-filled glove box. During the irradiation process, the sample was kept in the $-35\ °C$ Unisoku cryostat. Ten different (830, 785, 633, 532, 488, 442, 405, 355, 325, and 266 nm) laser lines were used. In addition to the above mentioned 785, 633, 532, and 488 nm lasers, Innovative Photonic Solutions 830 nm laser, Changchun New Industries optoelectronics 405, 355, and 266 nm lasers, Kimmon Koha Co., LTD. He-Cd IK 5751I-G 325/442 nm dual laser were used with the 50 % ND filter to reduce the power of lasers to 50 mW. The power of laser was measured before and after the reaction to ensure the stability, by using a Thorlabs PM160T laser power meter with a thermal sensor within 5 % measurement errors. For LED experiment, a 45 W 427 nm Kessil PR160L LED was placed 5 cm away from the samples.

To measure the yield of the C–Cl coupled product after confirming the complete decay of **1** with the ^{1}H-NMR spectroscopy, 3.6 equivalent of pyridine-d_5 was added to release the C−Cl coupled product from the Pd center, and after 2 hours, the final ^{1}H-NMR spectra were measured, as following the procedure reported previously.[2]

Protocol for ferrioxalate actinometry. Potassium ferrioxalate was synthesized as reported,[3] and samples for the irradiation process were prepared in the same way as **1**. 330 μL 6 mM potassium ferrioxalate solution was prepared with the 50 mM H_2SO_4 solution, and placed in a cuvette with 1 mm path length. After 50 mW 405 nm irradiation, 1 mL 0.1 % 1,10-phenanthroline (phen) aqueous solution and 125 μL 100 mM NaOAc/1 % H_2SO_4 aqueous solution were added to the 250 μL of the irradiated solution, and distilled water was filled to 2.5 mL. The final concentration was 0.6 mM, which is 10 times dilute relative to the solution irradiated. After waiting for 30 min, to quantify the $[Fe(phen)_3]^{2+}$ complex produced, the solution was placed in a 5 mm cuvette and the electronic absorption at 510 nm was measured. By using the extinction coefficient of 11,100 $M^{-1}cm^{-1}$ at 510 nm,[4] the photo-induced conversion ratios were calculated and compared to quantum yields reported in literature[3] to assess the effectiveness of our irradiation set-up.

Computational details. All the DFT calculations were conducted by the Gaussian 09-d.01[5] package, with B3LYP functional[6] in combination with 6-311g(d,p) basis set[7] for main group atoms and LANL2TZ(f) basis set[8] including effective core potential for Pd and Pt atoms obtained from the Basis Set Exchange software[9]. The CPCM solvation model was used with a dielectric constant of 36 for acetonitrile.[10] Mulliken population analysis and Mayer bond order calculations were performed with the QMForge 2.4 software.[11] The reaction coordinates were searched by calculating potential energy surfaces along the Pd–C and C–Cl bonds. Transition states were confirmed by one imaginary frequency and intrinsic reaction coordinate (IRC) calculations. Spin-orbit coupling constants of the Pd and Pt complexes were calculated by using the ORCA 4.2.0 software[12], utilizing the ZORA-DEF2-TZVP basis set[13] for main-group atoms and SARC-ZORA-TZVP basis set[14] for Pd and Pt atoms, along with the B3LYP functional[6].

Thermal reductive elimination reactions

(c)

T (K)	k (s^{-1})
278	$3.2\ (\pm 0.1) \times 10^{-4}$
283	$6.6\ (\pm 0.3) \times 10^{-4}$
288	$1.3\ (\pm 0.1) \times 10^{-3}$
293	$2.6\ (\pm 0.2) \times 10^{-3}$
298	$4.7\ (\pm 0.3) \times 10^{-3}$
303	$7.7\ (\pm 0.8) \times 10^{-3}$

(d) Slope = -10700 ± 300
y-intercept = 24.8 ± 0.8

(e)

	Activation barrier
$\Delta H^{\ddagger}$	21.2 ($\pm$ 0.6)
$\Delta S^{\ddagger}$	2 ($\pm$ 2)
$\Delta G^{\ddagger}_{298K}$	20.6 ($\pm$ 0.8)
$\Delta G^{\ddagger}_{238K}$	20.7 ($\pm$ 0.8)

Fig. S1 (a) Decay of **1** at −35 ℃ (black), 5 ℃ (red), 10 ℃ (orange), 15 ℃ (yellow), 20 ℃ (green), 25 ℃ (light blue), and 30 ℃ (blue), monitored by electronic absorption at 465 nm. (b) ln[**1**] as a function of reaction time. (c) Rate constants k's obtained from (b). (d) Eyring plot with k's in s^{-1}. (e) $\Delta H^{\ddagger}$ and $\Delta G^{\ddagger}$ in kcal/mol and $\Delta S^{\ddagger}$ in cal/mol K obtained from the Eyring plot. The k_{238K} of 2.9×10^{-5} min^{-1} was obtained from extrapolation.

# Photo-induced reductive elimination kinetics
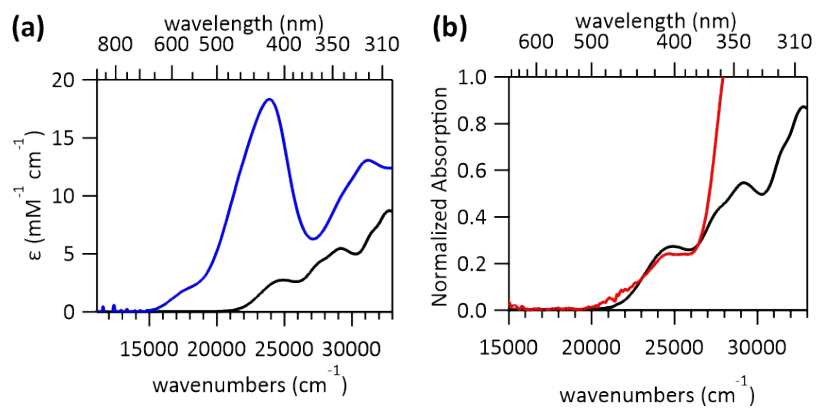
Fig. S2 (a) Abs spectra of **1** (blue) and [(phpy)Pd^{II}(OAc)]$_2$ (black). (b) Abs spectra of [(phpy)Pd^{II}(OAc)]$_2$ (black) and the final solution obtained after 442 nm laser irradiation onto **1** (red).
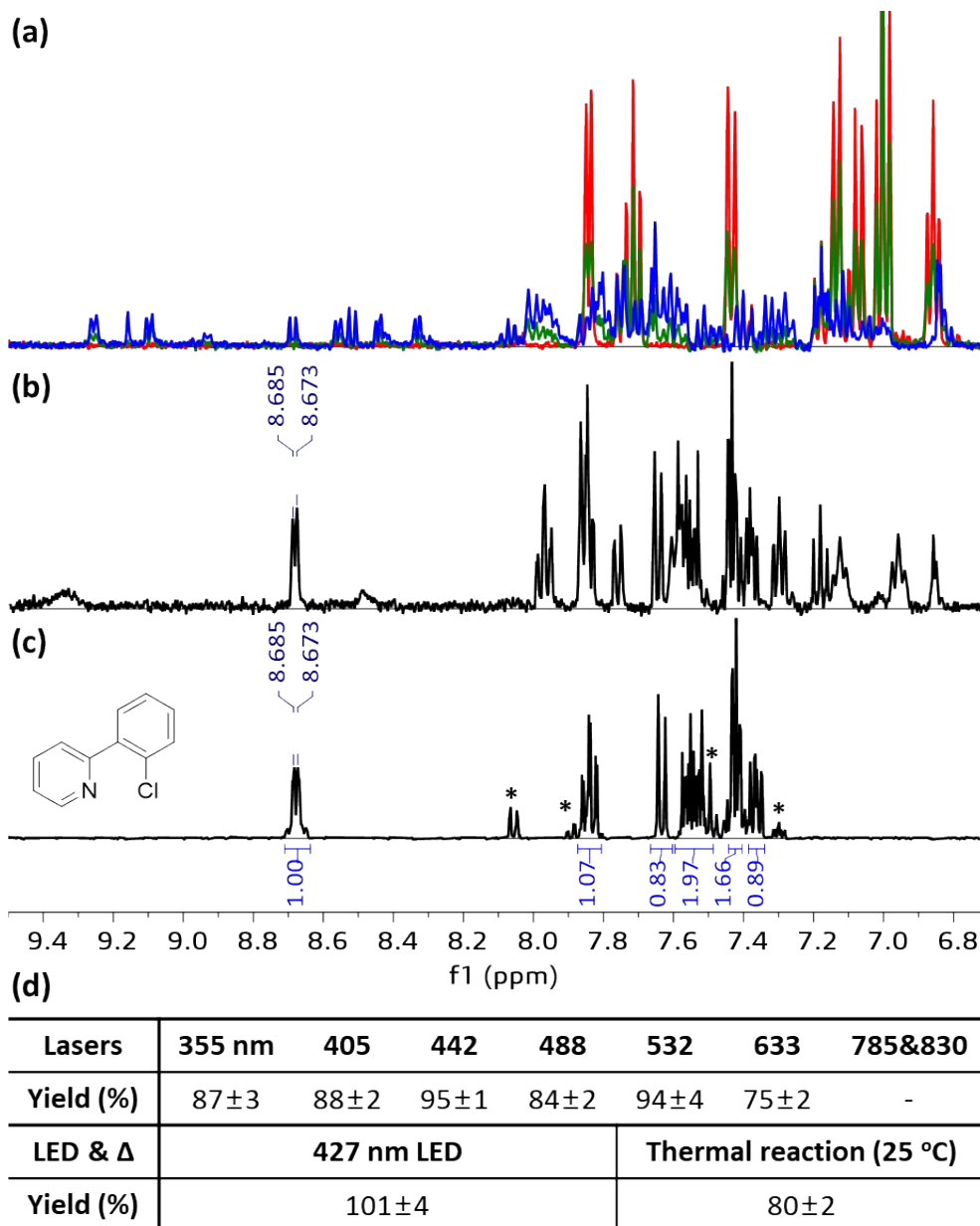
Fig. S3 ¹H NMR-monitored photochemical transformation of **1** with 442 nm laser irradiation. (a) Spectra obtained after 0 (red), 15 (green), and 60 min (blue) irradiation. (b) Final spectrum obtained 2 hours after addition of pyridine-d_5 to the irradiated solution. (c) Separately synthesized 2-(2-chlorophenyl)pyridine (**2**). Peaks labeled with asterisks are irrelevant side products from synthesis. (d) Yields of **2** from a thermal reaction at room temperature and photochemical reactions at −35 ℃ of **1**.
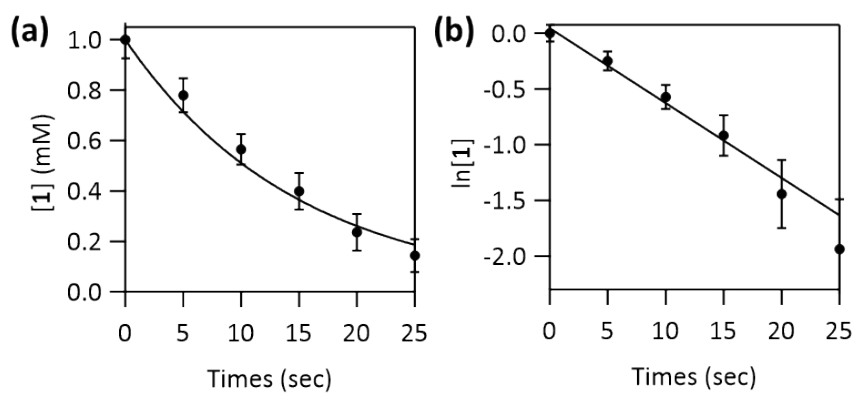
Fig. S4 (a) 45 W 427 nm LED induced decay of **1**. (b) The natural logarithm plot as a function of irradiation time at −35 ℃, showing the 1st order kinetics. The fit curve is obtained with k = 4.0 (± 0.5) min⁻¹.
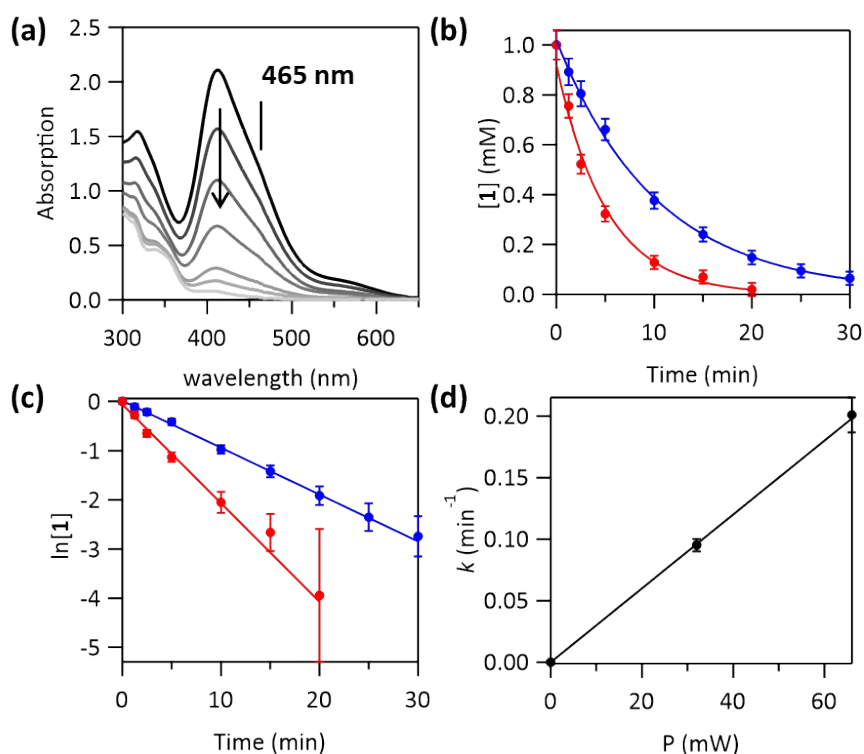
Fig. S5 Light power dependence of the photo-decay of **1**. (a) Abs spectra of **1** obtained 0, 1.25, 2.5, 5, 10, 15, and 20 minutes after 66 mW 442 nm l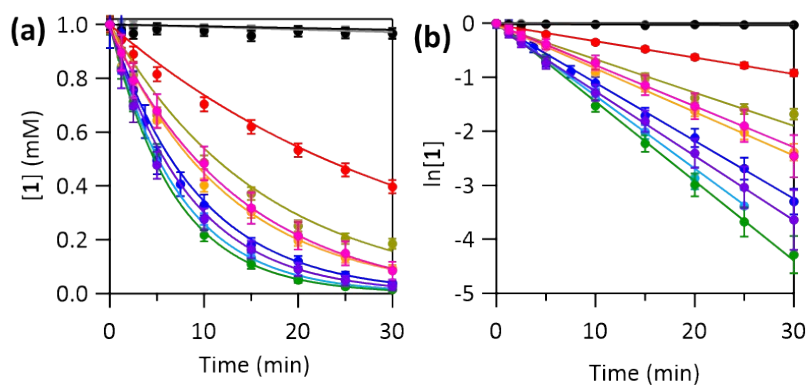aser irradiation**.** (b) [**1**] and (c) ln[**1**] versus irradiation time obtained. Decay of **1** with a power of 32 mW (blue) and 66 mW (red). (d) 1st order rate constants (*k*'s) versus laser power. This linear relationship was used for converting rate constants obtained with different laser powers to those of a normalized laser power of 50 mW.

Fig. S6 (a) Decay of **1** as a function of irradiation time of the 50 mW 830 (black), 785 (gray) 633 (red), 532 (orange), 488 (yellow), 442 (green), 405 (light blue), 355 (blue), 325 (purple), and 266 (pink) nm lasers. (b) Plots of ln[**1**] vs. irradiation time to show the 1st-order kinetics of the RE reaction. Rate constants obtained from (b) were used to construct the fitting curves in (a).

Table S1 1st-order rate constants (k, in min^{-1}) and quantum yields (Φ) for the photo-induced decay of **1** with 50 mW laser lines. Errors in k values obtained by linear regression analysis are represented.

	830 nm	785 nm	633 nm	532 nm	488 nm
k	7 ($\pm$7) $\times$ 10^{-4}	1.0 ($\pm$0.6) $\times$ 10^{-3}	3.0 ($\pm$0.2) $\times$ 10^{-2}	8.1 ($\pm$0.3) $\times$ 10^{-2}	6.0 ($\pm$0.2) $\times$ 10^{-2}
Φ	0	0.044	0.18	0.12	0.05
	442 nm	405 nm	355 nm	325 nm	266 nm
k	1.6 ($\pm$0.1) $\times$ 10^{-1}	1.3 ($\pm$0.1) $\times$ 10^{-1}	1.1 ($\pm$0.1) $\times$ 10^{-1}	1.2 ($\pm$0.1) $\times$ 10^{-1}	7.6 ($\pm$0.7) $\times$ 10^{-2}
Φ	0.12	0.12	0.13	0.14	0.10
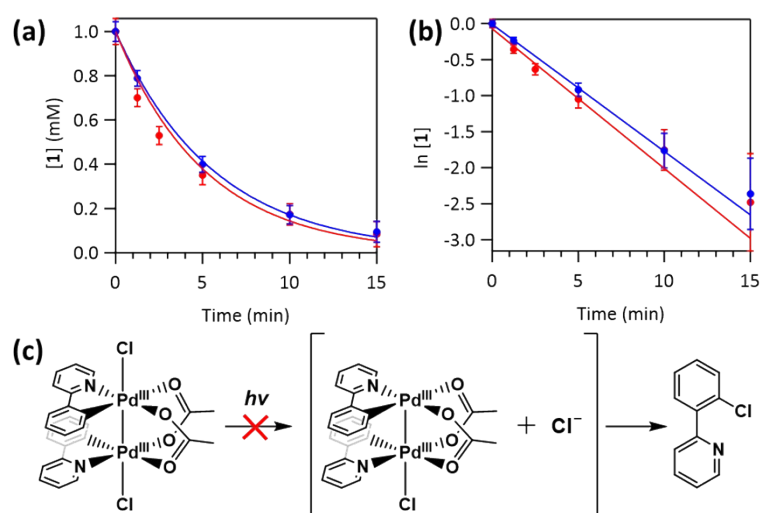
Fig. S7 Effect of exogenous Cl⁻ on the RE rate. (a) Decay of **1** as a function of irradiation time of the 50 mW 442 nm laser in the presence (blue) and absence (red) of 3 equivalents tetra-n-butylammonium chloride (TBACl). (b) Plots of ln[**1**] vs. irradiation time to show the 1st-order kinetics of the RE reaction. (c) Scheme for the RE reaction of **1** driven by photo-induced Cl⁻ dissociation which can be excluded by this experiment. Rate constants ($1.8 (\pm 0.1) \times 10^{-1}$ min⁻¹ for blue and $1.9 (\pm 0.2) \times 10^{-1}$ min⁻¹ for red) obtained from (b) were used to construct the fitting curves in (a).
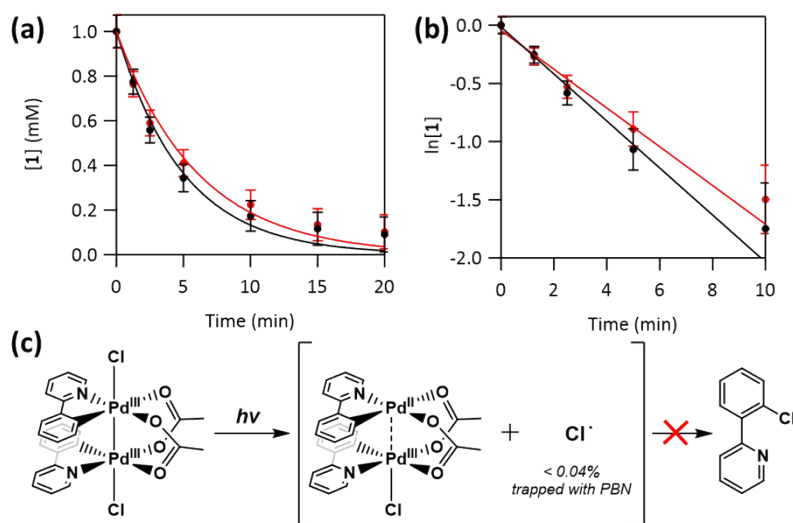
Fig. S8 Effect of exogenous α-phenyl-N-tert-butylnitrone (PBN) on the RE rate. (a) Decay of **1** as a function of irradiation time of the 50 mW 442 nm laser in the presence (black) and absence (red) of 50 equivalents PBN. (b) Plots of ln[**1**] vs. irradiation time to show the 1st-order kinetics of the RE reaction. (c) Scheme for the RE reaction of **1** driven by photo-induced Cl⁻ radical dissociation which can be excluded by this experiment. Rate constants ($2.0 (\pm 0.3) \times 10^{-1}$ min⁻¹ for black and $1.7 (\pm 0.2) \times 10^{-1}$ min⁻¹ for red) obtained from (b) were used to construct the fitting curves in (a).

- 11 -
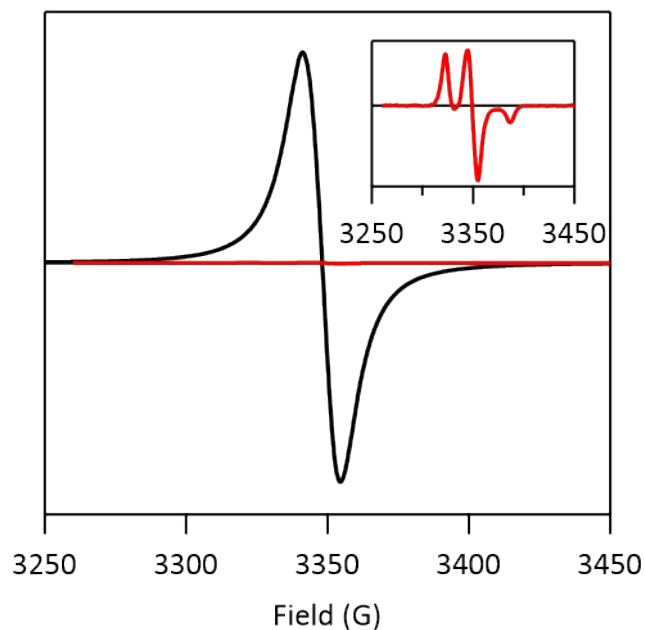
Fig. S9 100 K X-band EPR spectra of final solution after completing the photochemical RE reaction of **1** + 50 equivalents PBN with 427 nm LED at −35 ^{o}C (red). (2,2,6,6-tetramethylpiperidin-1-yl)oxyl (TEMPO) radical used as a spin quantification external standard (black). The inset describes a magnified spectrum. Based on the initial concentration of complex **1**, 0.04 % of PBN adduct was detected after finishing the RE reaction.

Raman spectra of Pd complexes
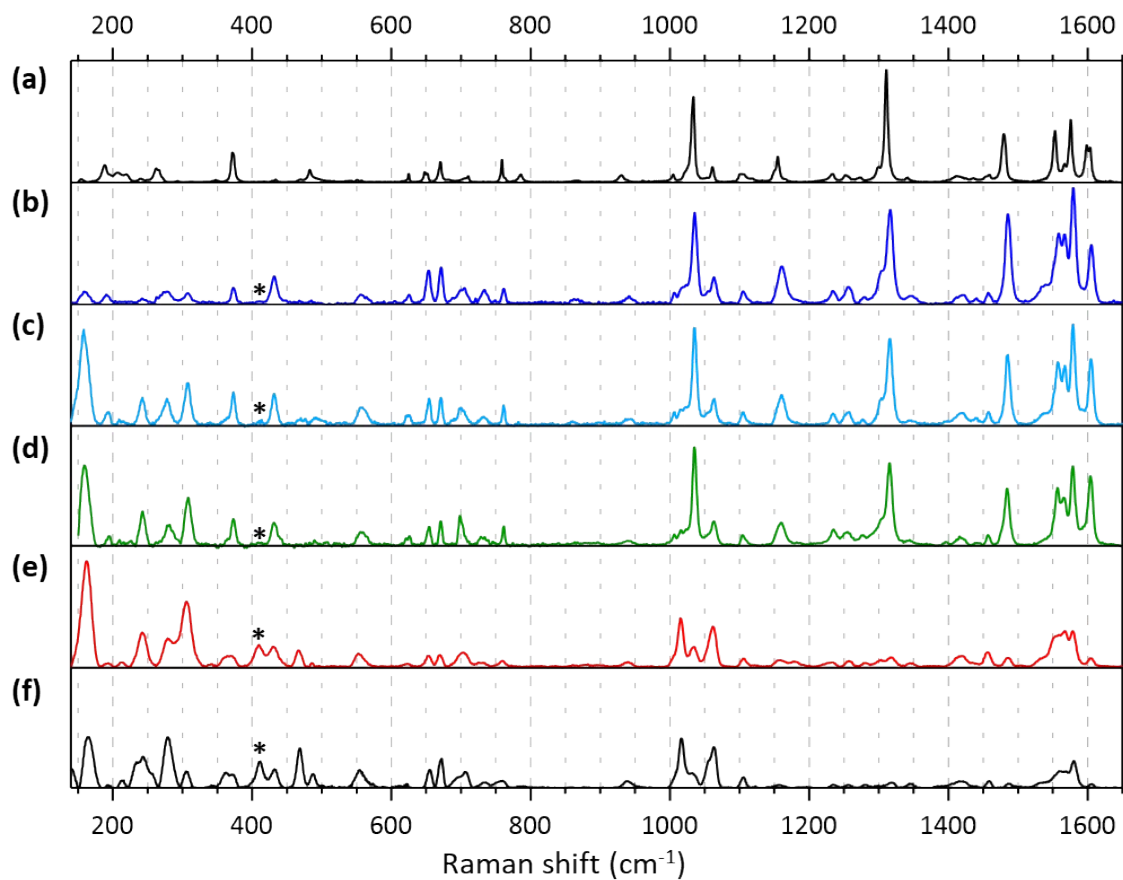
Fig. S10 (a) 298 K off-resonance Raman spectrum of [(phpy)Pd^{II}(OAc)]$_2$ measured with 532 nm laser excitation. (b)-(f) 77 K resonance Raman spectra of **1** measured with (b) 488, (c) 515, (d) 532, (e) 633, and (f) 785 nm laser excitations. Spectra in (e) and (f) were 10 times magnified for clarity. Asterisk-labeled peaks at 411 cm^{-1} were used for intensity normalization
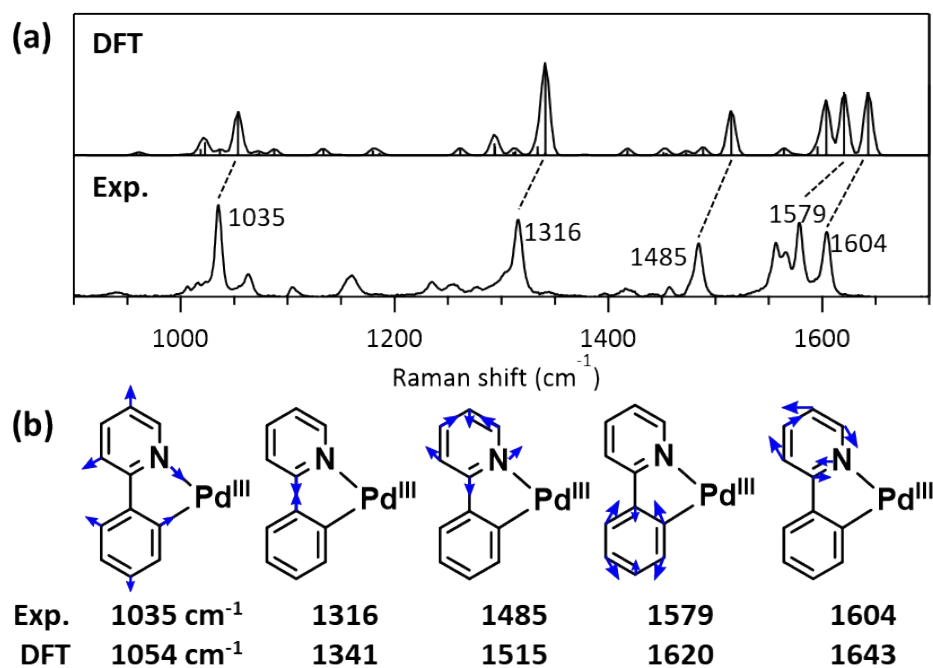
Fig. S11 (a) DFT-calculated and experimental Raman spectra of **1** obtained with 532 nm excitation. (b) DFT-calculated frequencies and normal modes that contain the C−C/C=C and C−N/C=N stretching vibrations of the phpy ligand. Negligible motions of other atoms are omitted for clarity.

Quantum yield determination by ferrioxalate actinometry

(a)

(b)

(c)

(d)

	v (M s^{-1})	Φ
1	1.6×10^{-6}	0.12
Ferrioxalate	1.5×10^{-5}	1.14
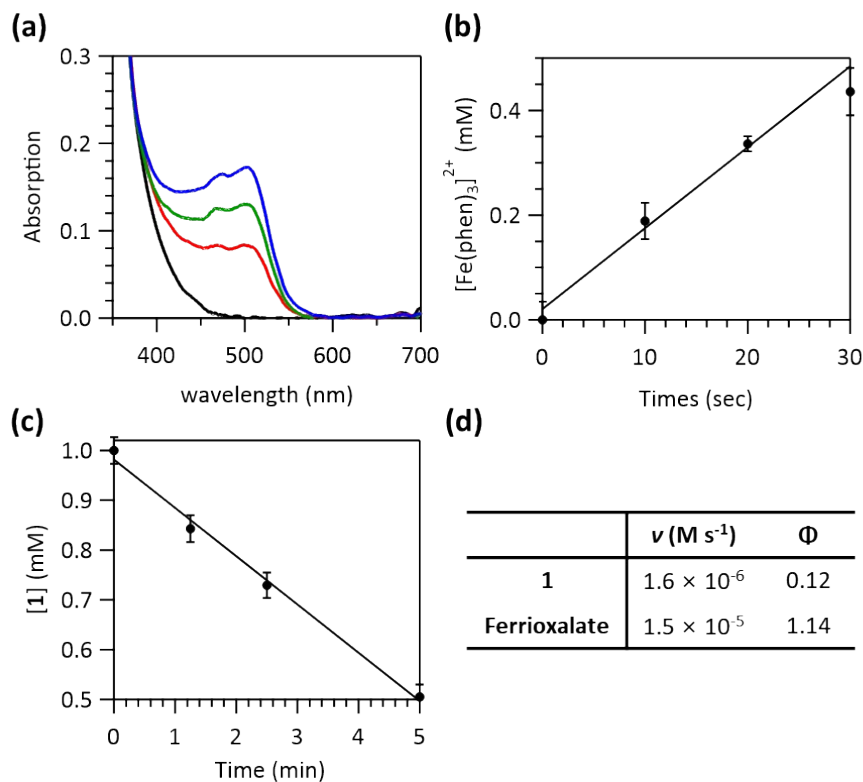
Fig. S12 Abs spectra obtained after adding 1,10-phenanthroline (phen) into the ferrioxalate solution that had been exposed to the 405 nm laser line for 0 (black), 10 (red), 20 (green), and 30 (blue) seconds. (b) Yield of $[Fe(phen)_3]^{2+}$ as a function of irradiation time. (c) Decay of **1** as a function of irradiation time. (d) Rates (v's) and quantum yields (Φ's) of photoreactions obtained by using the literature reported $\Phi_{ferrioxalate}$, and the equation of $\Phi_1 = v_1/v_{ferrioxalate} \times \Phi_{ferrioxalate}$.

Validation of DFT models

Table S2 Metal-ligand bond distances of **1** in the X-ray crystal structure[2] and the DFT-optimized structures obtained with the BP86,[6a, 15] B3LYP,[6] and Cam-B3LYP[16] functionals.

	Crystal	BP86	B3LYP	Cam-B3LYP
Pd–Pd	2.57	2.68	2.71	2.60
Pd–Cl	2.42	2.51	2.52	2.47
Pd–O$_{trans-to-N}$	2.04	2.07	2.06	2.04
Pd–O$_{trans-to-C}$	2.13	2.21	2.22	2.17
Pd–C	2.00	2.00	2.00	1.99
Pd–N	2.02	2.04	2.04	2.02
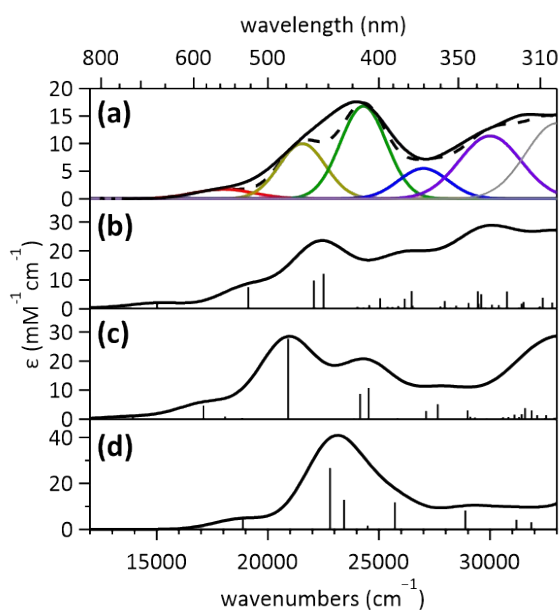
Fig. S13 (a) Experimental Abs spectrum of **1**, and TDDFT-simulated Abs spectra obtained with the (b) BP86, (c) B3LYP, and (d) Cam-B3LYP functionals. The B3LYP calculation was used for detailed analysis.

Table S3 Effects of a variation in the Pd–Cl bond length on metal-ligand bond distances and Gibbs free energy. Since DFT calculations tend to overestimate the Pd–Cl bond lengths, structures with the Pd–Cl bond lengths constrained were tested, showing that the constraints barely affect other bonds and energy.

	Full optimization	Pd–Cl Constrained optimization	
		2.46 Å	2.42 Å
Pd–Pd	2.71	2.71	2.72
Pd–Cl	2.52	2.46	2.42
Pd–$O_{trans-to-N}$	2.06	2.07	2.07
Pd–$O_{trans-to-C}$	2.22	2.22	2.22
Pd–C	2.00	2.00	2.00
Pd–N	2.04	2.04	2.05
ΔG_{243K}	0.00 kcal/mol	+0.65 kcal/mol	+1.65 kcal/mol
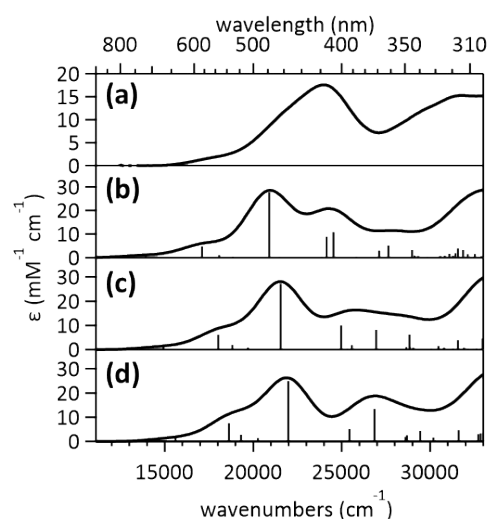
Fig. S14 (a) Experimental Abs spectrum of **1**, and TDDFT-simulated Abs spectra of **1** with (b) the fully-optimized Pd–Cl bond lengths of 2.52 Å and the constrained Pd–Cl bond lengths of (c) 2.46 Å and (d) 2.42 Å. The last spectrum from the most crystal-like structure best reproduces the experiment and thus was used for detailed analysis.
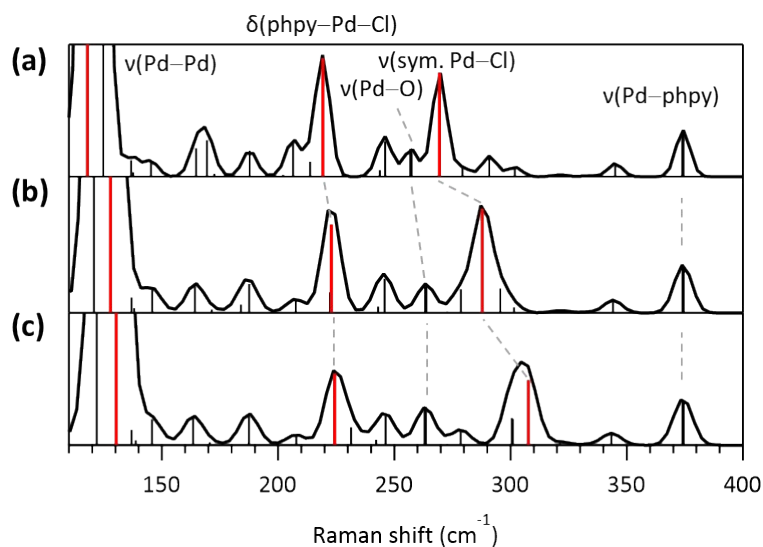
Fig. S15 Effects of a variation in the Pd–Cl bond length on DFT-calculated normal modes. DFT-simulated Raman spectra of **1** with the Pd–Cl bond lengths of (a) 2.52 Å, (b) 2.46 Å, and (c) 2.42 Å, showing that the energies of the Pd–Pd and Pd–Cl stretching vibrations can be significantly underestimated with the overestimated Pd–Cl bond lengths. The last spectrum obtained from the most crystal-like structure was used for detailed analysis.

Fit parameters and TDDFT assignments for the MCD/Abs spectra of 1

Table S4 Gaussian deconvolution fit parameters for the MCD and Abs spectra of **1**, and related TDDFT-calculated transitions.

Band	Abs		MCD		$10^5 \times$ MCD/Abs ratio	TDDFT assignment	
	Energy (cm^{-1})	ε (M^{-1}cm^{-1})	Energy (cm^{-1})	$\Delta\varepsilon$ (M^{-1}cm^{-1})			
1	18,000	1,700	17,700	−0.14	−8.2	**#3** 147 → 148 (34 %) 146 → 148 (56 %)	Pd$_2$ dσ → dσ*
2	21,550	10,000	21,200	−0.23	−2.3	**#10** 146 → 148 (37 %) 143 → 148 (32 %) 147 → 148 (21 %)	Phpy π → Pd$_2$ dσ*
3	24,300	16,800	24,600	−0.34	−2.0	**#19** 143 → 148 (53 %) 147 → 148 (25 %)	Phpy π → Pd$_2$ dσ*
4	27,000	5,500	27,200	+0.35	+6.4	**#30** 137 → 148 (74 %) 147 → 151 (17 %)	OAc 2p → Pd$_2$ dσ*
5	30,000	11,400	30,400	+1.22	+11	**#35** 147 → 151 (53 %) 137 → 148 (12 %)	Pd$_2$ dσ → d$_{x^2-y^2}$

Excited-state lifetimes of d^7-d^7 binuclear complexes and spin-orbit coupling (SOC) calculations

Table S5 Excited-state lifetimes of metal-metal bonded d^7-d^7 binuclear complexes in literature.[17]

Species	Excited-state lifetime
[Pt^{III}(μ-pyrophosphite)$_2$X]$_2$[17a]	22 μs (X = Cl, 77 K)
	15 μs (X = Br, 77 K)
	18 μs (X = SCN, 77 K)
	23 μs (X = py, 77 K)
[Re^0(bis(dimethylphosphino)methane)(CO)$_3$]$_2$[17b]	31 μs (77 K)
[Rh^{II}(μ-acetate)$_2$(L)]$_2$[17c]	4.4 μs (L = MeOH)
	5.0 μs (L = PPh$_3$)
	3.5 μs (L = THF)
	4.8 μs (L = py)
[Pt^{III}(μ-C$_6$H$_3$-5-Me-2-AsPh$_2$)$_2$(CN)]$_2$[17d]	30 μs (77 K)

Table S6 TDDFT-calculated spin-orbit coupling (SOC) between the singlet and triplet excited states of the $(d\sigma)^1(d\sigma^*)^1$ configuration of **1** and benchmark systems, [Pt^{III}(μ-pyrophosphite; pop)$_2$Cl]$_2$ and [Re^0(bis(dimethylphosphino)methane; dmpm)(CO)$_3$]$_2$, which are known to undergo ISC to the triplet state.[17a, 17b]
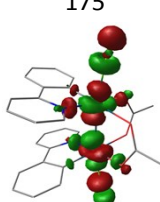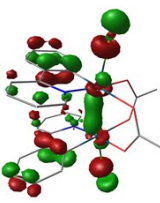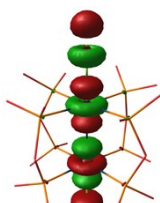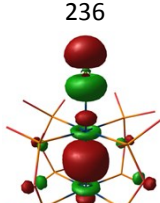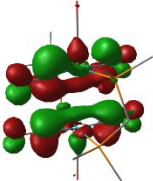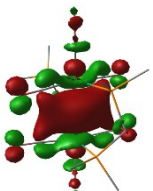
Species	Excited state	TDDFT assignment	Molecular orbitals (MO)	DFT-calculated SOC constants
[Pd^{III}(phpy)(OAc)Cl]$_2$ (1)	Singlet $(d\sigma)^1(d\sigma^*)^1$	MO #174 → #175 (64 %) (12,396 cm^{-1})	175 174	22.2
	Triplet $(d\sigma)^1(d\sigma^*)^1$	MO #174 → #175 (59 %) (4,807 cm^{-1})		
[Pt^{III}(pop)$_2$Cl]$_2$	Singlet $(d\sigma)^1(d\sigma^*)^1$	MO #236 → #241 (69 %) (30,916 cm^{-1})	241 236	23.1
	Triplet $(d\sigma)^1(d\sigma^*)^1$	MO #236 → #241 (97 %) (17,734 cm^{-1})		

Table S6. Continued.

Species	Excited state	TDDFT assignment	Molecular orbitals (MO)	DFT-calculated SOC constants
$[Re^0(dmpm)(CO)_3]_2$	**Singlet** $(d\sigma)^1(d\sigma^*)^1$	MO #190 → #193 (48 %) (30,064 cm^{-1})	193	845
	Triplet $(d\sigma)^1(d\sigma^*)^1$	MO #190 → #193 (71 %) (23,404 cm^{-1})	190	

Comparison of internal charge transfer energies
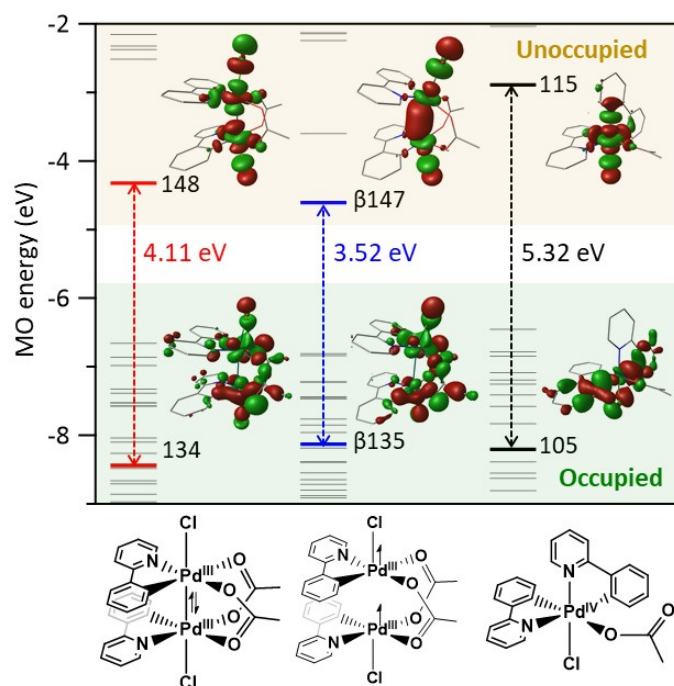
Fig. S16 The comparison of DFT-calculated MO energy plot showing internal charge transfer (ICT) energies relevant to RE reactions of **1**(S_0) (left), **1**(T_1) (middle), and (phpy)$_2$Pd^{IV}(OAc)Cl (right).

DFT-calculated RE reactions of 1 at the ground and triplet excited states

	S_0	T_1
Pd—Pd	2.71 Å	3.14 Å
Pd—Cl	2.52 Å	2.56 Å
Pd—C	2.00 Å	1.99 Å
Pd—N	2.04 Å	2.07 Å
Pd—O$_{trans-to-C}$	2.22 Å	2.22 Å
Pd—O$_{trans-to-N}$	2.06 Å	2.08 Å
∠ Pd—Pd—Cl	170°	162°
ΔE (kcal/mol)	0.0	+6.6
ΔH (kcal/mol)	0.0	+6.2
ΔG$_{243K}$ **(kcal/mol)**	0.0	+3.1
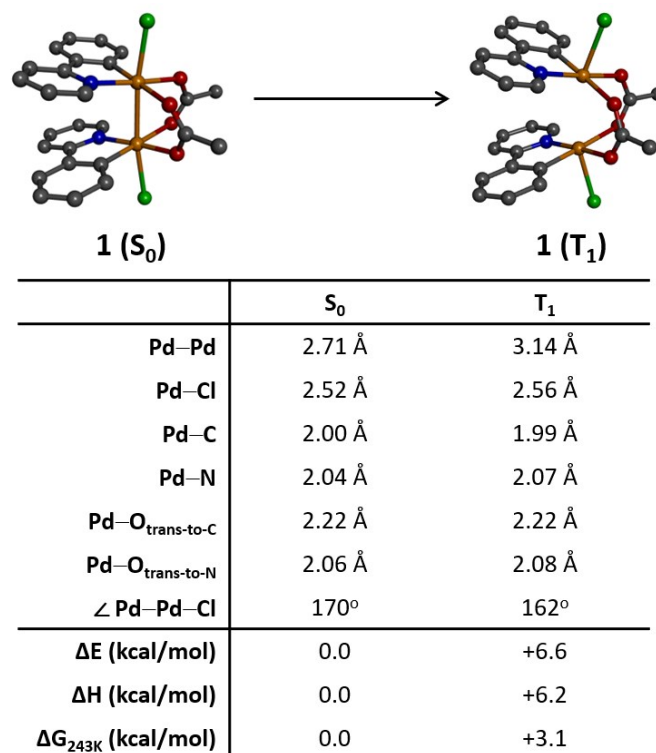
Fig. S17 DFT-calculated relative energies and geometries of **1** at the ground state (S_0) and the triplet excited state (T_1).
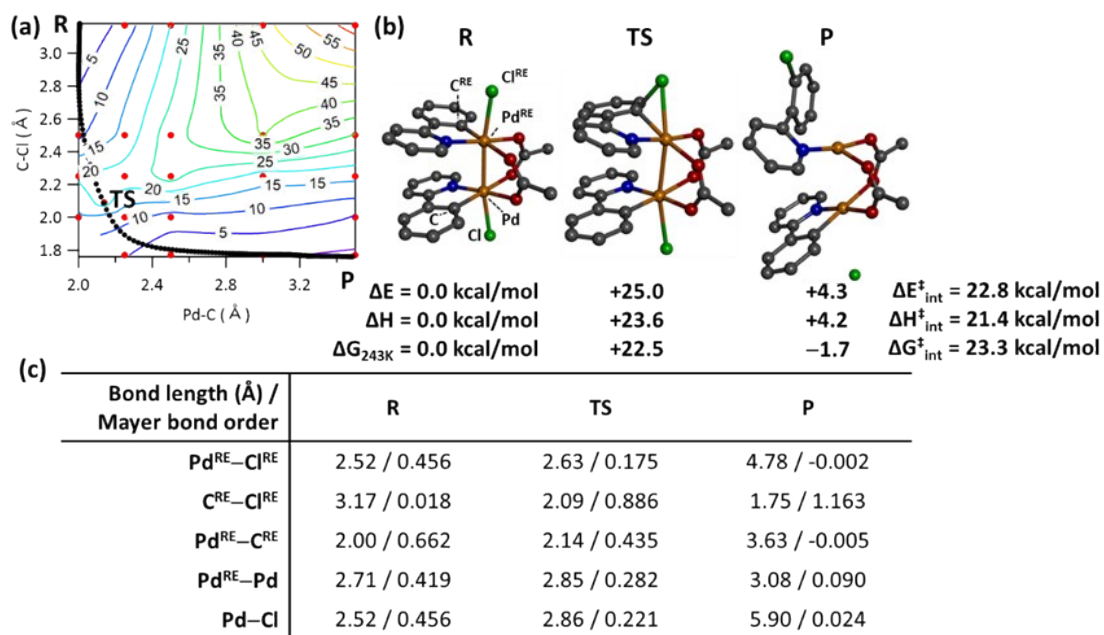
Fig. S18 (a) Potential energy surface for the C−Cl bond-forming RE reaction of **1** at the ground state (S$_0$). (b) Energy and (c) bond length changes from reactant (R) to the transition state (TS) and product (P).

Bond length (Å) / Mayer bond order	R	TS	P
Pd^{RE}−Cl^{RE}	2.52 / 0.456	2.63 / 0.175	4.78 / -0.002
C^{RE}−Cl^{RE}	3.17 / 0.018	2.09 / 0.886	1.75 / 1.163
Pd^{RE}−C^{RE}	2.00 / 0.662	2.14 / 0.435	3.63 / -0.005
Pd^{RE}−Pd	2.71 / 0.419	2.85 / 0.282	3.08 / 0.090
Pd−Cl	2.52 / 0.456	2.86 / 0.221	5.90 / 0.024

ΔE = 0.0 kcal/mol, +25.0, +4.3, ΔE$^{‡}_{int}$ = 22.8 kcal/mol
ΔH = 0.0 kcal/mol, +23.6, +4.2, ΔH$^{‡}_{int}$ = 21.4 kcal/mol
ΔG$_{243K}$ = 0.0 kcal/mol, +22.5, −1.7, ΔG$^{‡}_{int}$ = 23.3 kcal/mol
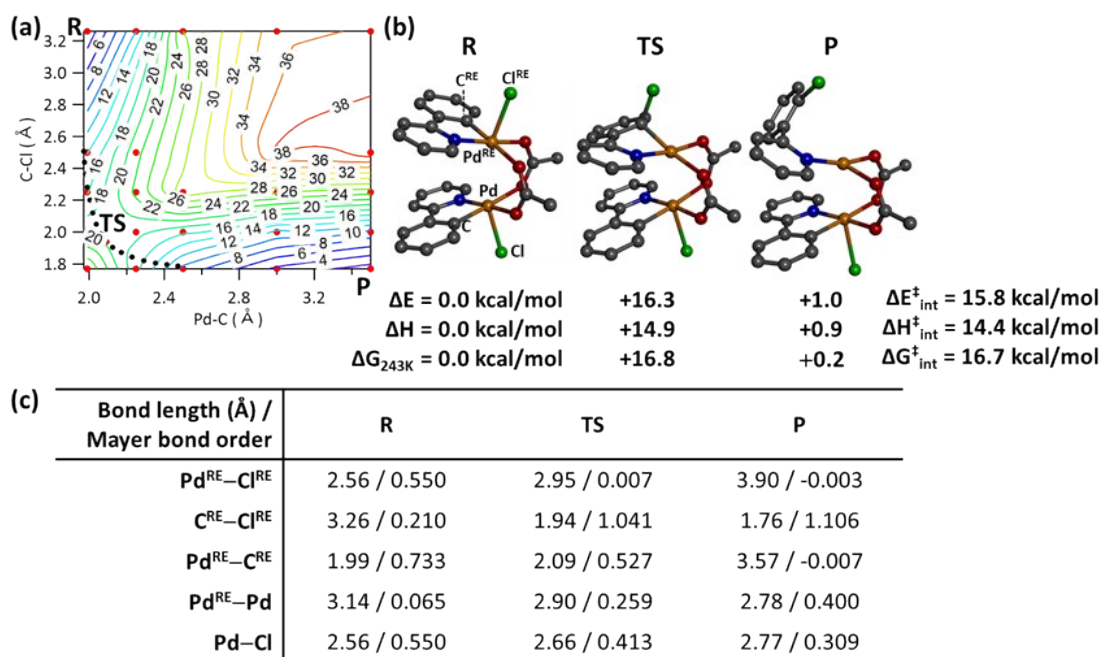
Fig. S19 (a) Potential energy surface for the C−Cl bond-forming RE reaction of **1** at the T$_1$ state. (b) Energy and (c) geometry changes from reactant (R) to the transition state (TS) and product (P).

Bond length (Å) / Mayer bond order	R	TS	P
Pd^{RE}−Cl^{RE}	2.56 / 0.550	2.95 / 0.007	3.90 / -0.003
C^{RE}−Cl^{RE}	3.26 / 0.210	1.94 / 1.041	1.76 / 1.106
Pd^{RE}−C^{RE}	1.99 / 0.733	2.09 / 0.527	3.57 / -0.007
Pd^{RE}−Pd	3.14 / 0.065	2.90 / 0.259	2.78 / 0.400
Pd−Cl	2.56 / 0.550	2.66 / 0.413	2.77 / 0.309

ΔE = 0.0 kcal/mol, +16.3, +1.0, ΔE$^{‡}_{int}$ = 15.8 kcal/mol
ΔH = 0.0 kcal/mol, +14.9, +0.9, ΔH$^{‡}_{int}$ = 14.4 kcal/mol
ΔG$_{243K}$ = 0.0 kcal/mol, +16.8, +0.2, ΔG$^{‡}_{int}$ = 16.7 kcal/mol

Table S7 Experimental and DFT-calculated $\Delta G^{\ddagger}_{243K}$'s for the RE reaction of **1** at the S_0 state, obtained with various functionals.

	Experimental	B3LYP	BP86	Cam-B3LYP
$\Delta G^{\ddagger}_{243K}$ (kcal/mol)	20.7	22.5	24.2	22.4

^{1}H-NMR spectra of Pd complexes
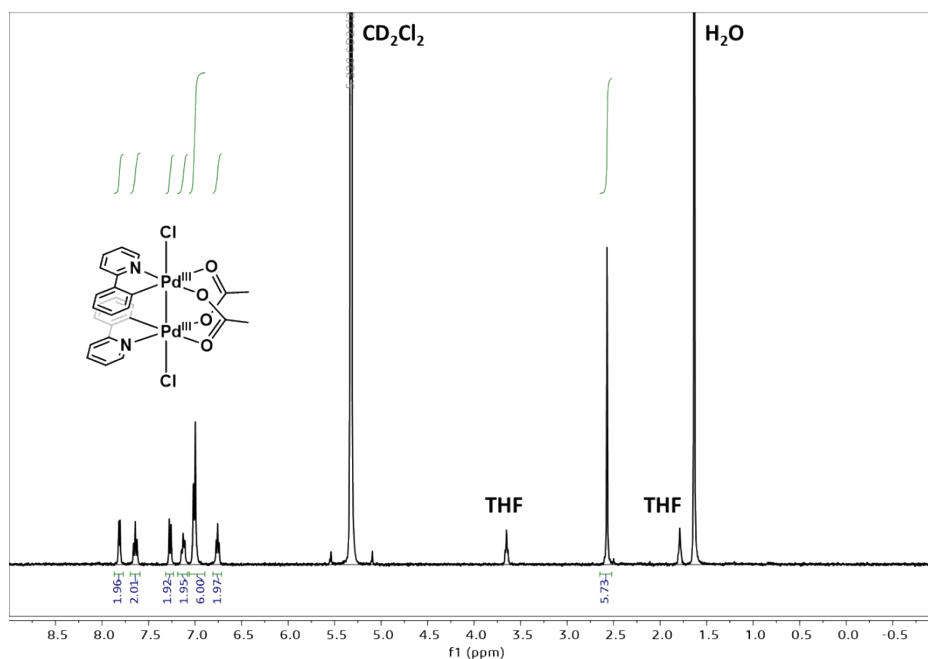
Fig. S20 ^{1}H-NMR spectrum of [(phpy)Pd^{III}(OAc)Cl]$_2$ in CD$_2$Cl$_2$. ^{1}H NMR (400 MHz, CD$_2$Cl$_2$, −30 °C): δ = 7.81 (d, J = 5.7 Hz, 2H, phpy), 7.64 (t, J = 7.8 Hz, 2H, phpy), 7.27 (d, J = 7.5 Hz, 2H, phpy), 7.15-7.09 (m, 2H), 7.04-6.98 (m, 6H, phpy), 6.76 (t, J = 6.4 Hz, 2H, phpy), 2.57 ppm (s, 6H, OAc).
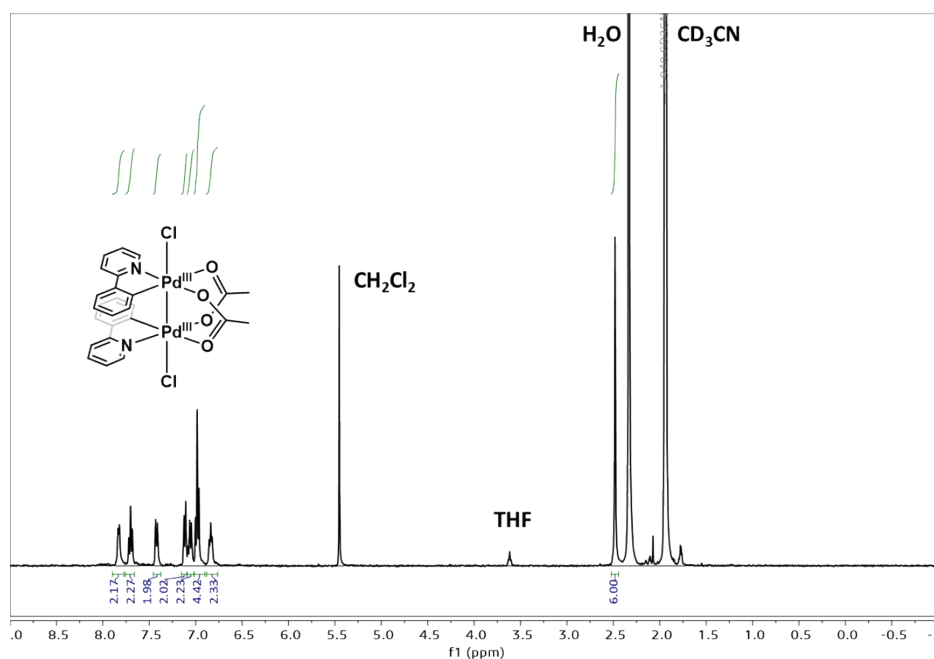
Fig. S21 ^{1}H-NMR spectrum of [(phpy)Pd^{III}(OAc)Cl]$_2$ in CD$_3$CN. ^{1}H NMR (400 MHz, CD$_3$CN, −30 °C): δ = 7.83 (d, J = 5.9 Hz, 2H, phpy), 7.70 (t, J = 7.7 Hz, 2H, phpy), 7.42 (d, J = 8.0 Hz, 2H, phpy), 7.12 (d, J = 7.5 Hz, 2H, phpy), 7.09-7.03 (m, 2H, phpy), 6.98 (t, J = 7.6 Hz, 4H, phpy), 6.84 (t, J = 7.4 Hz, 2H, phpy), 2.48 ppm (s, 6H, OAc).

Simulation for the dark reaction of 1

(a)

$R(S_0)$ $\xrightarrow[k_r]{k_f}$ $R(T_1)$

$\downarrow k_{S0}$ $\downarrow k_{T1}$

P from S$_0$ **P from T$_1$**
$P(S_0)$ $P(T_1)$

(b)

TS(S$_0$)
TS(T$_1$)
R(T$_1$) 16.8 22.5
R(S$_0$) 3.1

(c)

Eyring Equations

$$k_{S_0} = \frac{k_B T}{h} e^{-\frac{22.5}{RT}} = 2.92 \times 10^{-8}\ \text{min}^{-1}$$

$$k_{T_1} = \frac{k_B T}{h} e^{-\frac{16.8}{RT}} = 3.92 \times 10^{-3}\ \text{min}^{-1}$$

Boltzmann Factor

$$\frac{[R_{T_1}]}{[R_{S_0}]} = \frac{k_f}{k_r} = e^{-\frac{3.1}{RT}} = 1.63 \times 10^{-3}$$

Rate Equations

$$-\frac{d[R_{S_0}]}{dt} = -(k_{S_0} + k_f)[R_{S_0}] + k_r[R_{T_1}], \quad -\frac{d[P_{S_0}]}{dt} = k_{S_0}[R_{S_0}]$$

$$-\frac{d[R_{T_1}]}{dt} = -(k_{T_1} + k_r)[R_{T_1}] + k_f[R_{S_0}], \quad -\frac{d[P_{T_1}]}{dt} = k_{T_1}[R_{T_1}]$$

(d) **(e)** **(f)**

Concentration (%) vs Time (min)
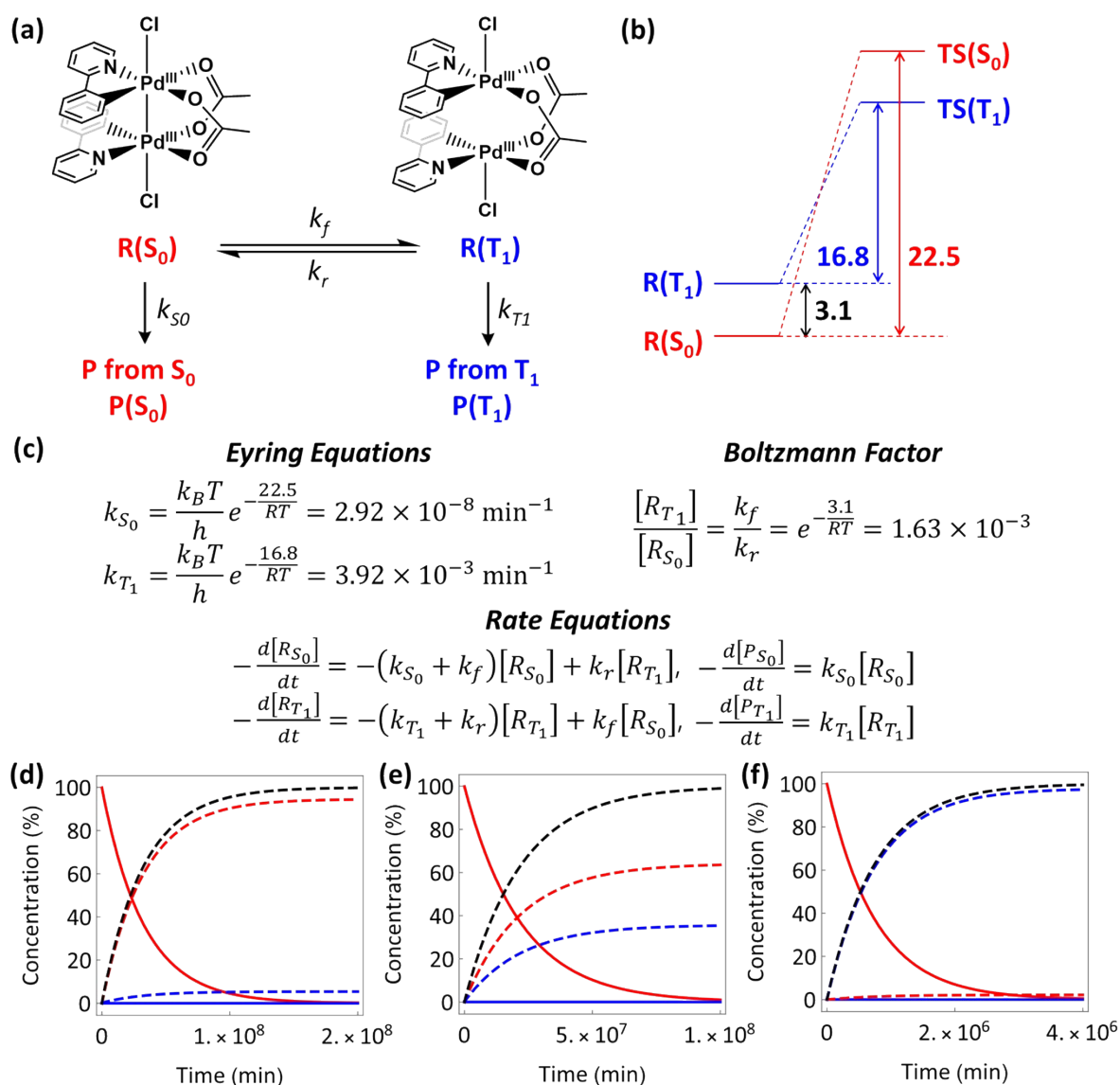
Fig. S22 Simulation for the dark reaction kinetics involving two electronic states, S$_0$ and T$_1$. (a) RE reaction scheme of **1** from S$_0$ and T$_1$ states with RE rate constants (k_{S0} and k_{T1}) and interconversion rate constants (k_f and k_r). (b) DFT-calculated ΔG values in kcal/mol. (c) Equations used for simulation of (d)~(f), including Eyring equations for determining k_{S0} and k_{T1} values, Boltzmann factor for determining the population ratio of the reactants in the S$_0$ vs. T$_1$ state (R(S$_0$) and R(T$_1$), respectively), and rate equations of reactions in scheme (a). (d)-(f) Simulated concentration changes of R(S$_0$) (red solid), R(T$_1$) (blue solid), the product from the S$_0$ pathway (P(S$_0$), red dashed), the product from the T$_1$ pathway (P(T$_1$), blue dashed), and P(S$_0$)+P(T$_1$) (black solid) when (d) the spin crossover is slower than the S$_0$ RE reaction with $k_f = 1.63 \times 10^{-9}$ min^{-1} and $k_r = 1.00 \times 10^{-6}$ min^{-1}, (e) the rate of spin crossover is comparable to that of the S$_0$ RE reaction with $k_f = 1.63 \times 10^{-8}$ min^{-1} and $k_r = 1.00 \times 10^{-5}$ min^{-1}, and (f) the spin crossover is faster than the S$_0$ RE reaction with $k_f = 1.63 \times 10^{-6}$ min^{-1} and $k_r = 1.00 \times 10^{-3}$ min^{-1} as a function of reaction time at 243 K.

Correlations between the ICT energy costs and C-C bond-forming RE reaction coordinate of Pt^{IV} complexes
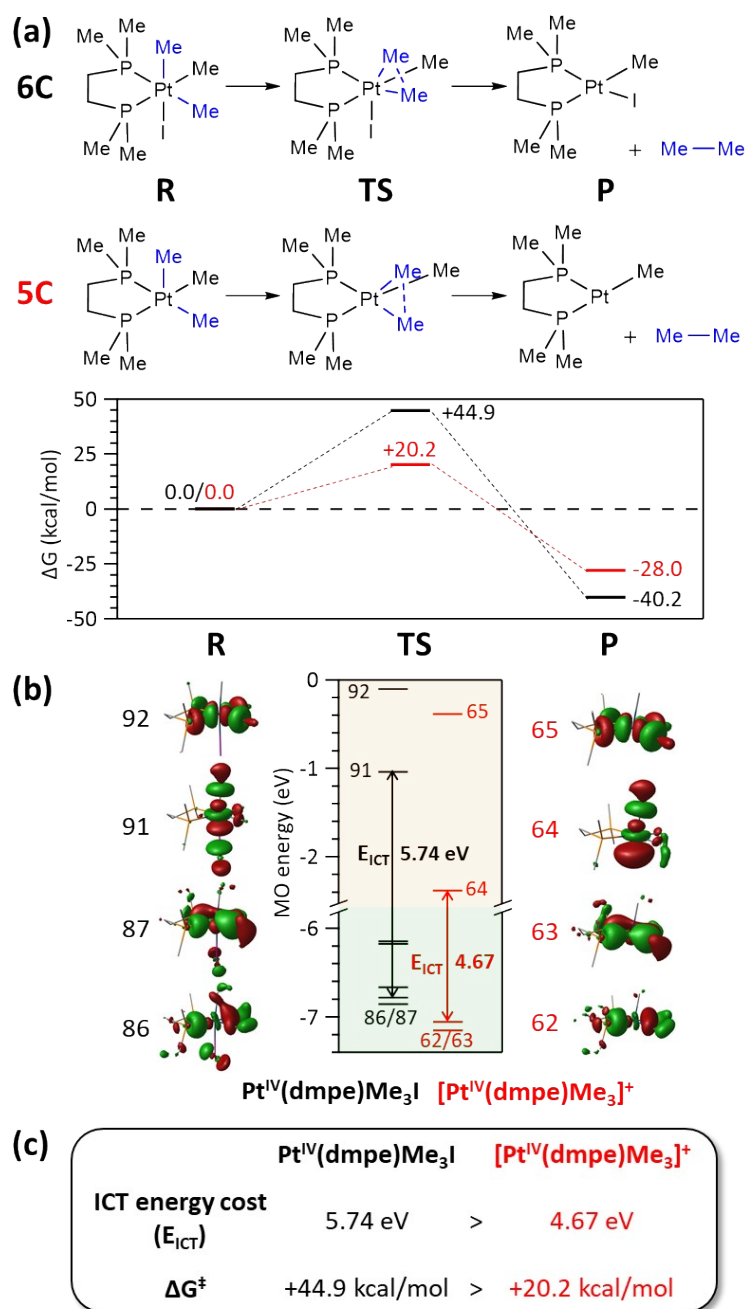
Fig. S23 (a) DFT-calculated RE reaction coordinate of 6C Pt^{IV}(1,2-bis(dimethylphosphino)ethane; dmpe)Me$_3$I (top) and 5C [Pt^{IV}(dmpe)Me$_3$]$^+$ (bottom) complexes. (b) FMOs and ICT energy costs of the RE reactions. (c) A comparison between the ICT energy costs and RE barriers of the 6C vs. 5C Pt^{IV} complexes.

Cartesian Coordinates of DFT-optimized Pd complexes

[(phpy)Pd^{III}(OAc)Cl]$_2$ (1), S$_0$

[(phpy)Pd^{III}(OAc)Cl]$_2$ (1), S$_0$
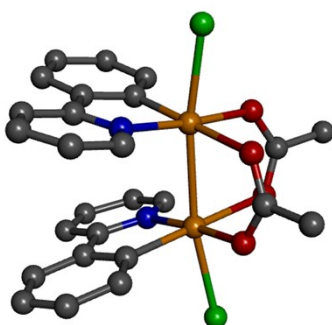
Pd	1.064645	1.269395	0.469346	C	-1.69526	-1.99571	-0.1859
N	-0.37899	1.024385	1.894874	C	-1.62125	-1.44322	-1.53629
C	-0.12522	0.577127	3.13209	O	2.452357	-1.67388	1.003225
C	-1.12512	0.492248	4.086994	O	2.715564	0.445999	1.702368
C	-2.41609	0.883435	3.738006	C	3.027749	-0.7688	1.699025
C	-2.66439	1.365117	2.460345	C	4.177658	-1.23205	2.56072
C	-2.85268	2.528029	-0.39898	Cl	1.493656	-3.56739	-1.41092
C	-2.79112	3.103266	-1.66319	H	0.896692	0.294492	3.339205
C	-1.57808	3.159335	-2.35037	H	-0.8893	0.123122	5.075679
C	-0.41397	2.627697	-1.7858	H	-3.22136	0.822093	4.459532
C	-0.48888	2.041667	-0.53429	H	-3.68729	3.51641	-2.10992
C	-1.69505	1.99587	0.185921	H	-1.53055	3.618504	-3.3313
C	-1.62107	1.44342	1.536326	H	0.526549	2.678473	-2.3178
O	2.452487	1.673648	-1.00327	H	5.100828	1.131509	-1.98295
O	2.715471	-0.44625	-1.70243	H	4.057818	2.278015	-2.83744
C	3.027753	0.768522	-1.69911	H	4.258357	0.605292	-3.4483
C	4.177605	1.231675	-2.56093	H	0.896591	-0.29448	-3.33918
Cl	1.494027	3.567231	1.410862	H	-0.88943	-0.12284	-5.0756
Pd	1.064507	-1.26952	-0.46936	H	-3.22155	-0.82159	-4.45943
N	-0.37913	-1.02431	-1.89485	H	-3.68761	-3.51614	2.109913
C	-0.12535	-0.57702	-3.13206	H	-1.53085	-3.61851	3.331248
C	-1.12526	-0.49199	-4.08693	H	0.526322	-2.67866	2.317734
C	-2.41627	-0.88306	-3.73793	H	5.100767	-1.13244	1.98246

C	-2.66459	-1.36477	-2.46028	H	4.057565	-2.27826	2.837615
C	-2.85293	-2.52777	0.399001	H	4.258862	-0.6054	3.447856
C	-2.7914	-3.10307	1.663181	H	-3.79585	2.503467	0.133775
C	-1.57836	-3.1593	2.350341	H	-3.65647	1.690804	2.180259
C	-0.4142	-2.62776	1.785763	H	-3.6567	-1.69036	-2.18018
C	-0.48908	-2.04166	0.534286	H	-3.79612	-2.50309	-0.13373

[(phpy)Pd^{III}(OAc)Cl]₂ (1), T₁
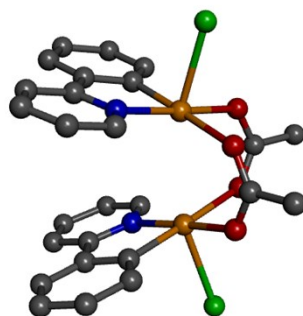
Pd	1.063416	1.479589	0.53003	C	-1.59384	-2.49053	-0.13627
N	-0.49959	1.322902	1.876965	C	-1.67151	-1.87146	-1.46034
C	-0.3943	0.746013	3.080912	O	2.519881	-1.72919	0.938842
C	-1.47623	0.672872	3.945524	O	2.522333	0.369229	1.778835
C	-2.69218	1.216838	3.537944	C	2.942308	-0.81246	1.717257
C	-2.791	1.821643	2.291303	C	4.074852	-1.20416	2.643799
C	-2.66524	3.111315	-0.51871	Cl	1.815714	-3.66293	-1.6371
C	-2.47505	3.697075	-1.76642	H	0.578834	0.348372	3.33494
C	-1.2168	3.673243	-2.36768	H	-1.36028	0.199884	4.911111
C	-0.13576	3.057013	-1.72888	H	-3.5568	1.174644	4.188813
C	-0.33278	2.460004	-0.49283	H	-3.30716	4.17729	-2.26706
C	-1.59364	2.49068	0.136288	H	-1.06922	4.136618	-3.33674
C	-1.67132	1.871636	1.460362	H	0.841442	3.04703	-2.19295
O	2.519989	1.72897	-0.93895	H	5.007464	0.80175	-2.2382
O	2.522289	-0.36945	-1.77894	H	4.163215	2.285679	-2.7239
C	2.942343	0.812211	-1.71737	H	3.919932	0.759422	-3.62742
C	4.074888	1.203825	-2.64395	H	0.578733	-0.34844	-3.33501
Cl	1.816037	3.66276	1.636996	H	-1.36044	-0.19972	-4.91109
Pd	1.063308	-1.4797	-0.53011	H	-3.55704	-1.17423	-4.1887
N	-0.49973	-1.32286	-1.87699	H	-3.30743	-4.17698	2.26713
C	-0.39443	-0.74597	-3.08094	H	-1.06945	-4.13655	3.336715
C	-1.47639	-0.6727	-3.9455	H	0.841281	-3.04715	2.192861
C	-2.69239	-1.21653	-3.53787	H	5.007461	-0.80226	2.23795
C	-2.79122	-1.82134	-2.29123	H	4.163026	-2.28602	2.72384
C	-2.66547	-3.11105	0.518764	H	3.920026	-0.75964	3.627238

C	-2.4753	-3.69685	1.76646	H	-3.64523	3.141712	-0.0573
C	-1.21702	-3.67315	2.36767	H	-3.72645	2.255065	1.965319
C	-0.13594	-3.05703	1.728828	H	-3.7267	-2.25465	-1.9652
C	-0.33295	-2.45999	0.492788	H	-3.64549	-3.14134	0.057389

(phpy)₂Pd^IV(OAc)Cl
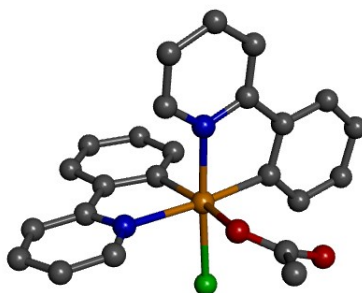
Pd	0.06132	-0.16541	-0.6628		H	-4.38187	-2.939	-1.46375
N	0.790901	-1.23856	0.942215		C	-4.71325	-1.2594	-0.13641
N	-2.02098	-0.78911	-0.44729		H	-5.77381	-1.44095	-0.01039
C	0.057901	-2.0979	1.664597		C	-4.11426	-0.18385	0.50706
H	-0.9888	-2.17734	1.411116		H	-4.70596	0.473449	1.128656
C	0.616746	-2.84707	2.686542		C	-2.74495	0.0422	0.336137
H	-0.00473	-3.52913	3.250302		C	-1.97606	1.145683	0.936779
C	1.975287	-2.69574	2.957432		C	-2.54802	2.071943	1.822649
H	2.444263	-3.26772	3.748471		H	-3.59171	1.985115	2.099141
C	2.726665	-1.80596	2.204887		C	-1.78912	3.106086	2.356966
H	3.78232	-1.68019	2.400139		H	-2.24554	3.812583	3.039863
C	2.117285	-1.07005	1.1851		C	-0.44556	3.229507	2.011828
C	2.773134	-0.09989	0.313252		H	0.152459	4.035091	2.422971
C	4.123659	0.266383	0.425674		C	0.144789	2.316029	1.133268
H	4.752992	-0.18776	1.181727		H	1.188032	2.429996	0.87348
C	4.6595	1.220481	-0.42868		C	-0.61225	1.281869	0.600671
H	5.701316	1.503216	-0.33709		O	0.368795	-1.95388	-1.83118
C	3.851956	1.817502	-1.39808		C	1.188417	-2.20686	-2.80386
H	4.267199	2.566944	-2.06292		O	2.054982	-1.45874	-3.25017
C	2.508352	1.458678	-1.52603		C	0.981077	-3.5996	-3.40508
H	1.894354	1.924101	-2.28414		H	-0.00371	-3.65086	-3.8774
C	1.973954	0.50025	-0.67732		H	1.748514	-3.8108	-4.14926
C	-2.59201	-1.82143	-1.07698		H	1.006703	-4.35934	-2.6208
H	-1.92265	-2.41643	-1.68663		Cl	-0.66204	1.154619	-2.50322
C	-3.94586	-2.09561	-0.94515					

References

1. X. F. Zhao and C. Zhang, *Synthesis*, 2007, 551-557.
2. D. C. Powers and T. Ritter, *Nat. Chem.*, 2009, **1**, 302-309.
3. C. G. Hatchard and C. A. Parker, *Proc. R. Soc. London Ser. A*, 1956, **235**, 518-536.
4. J. N. Demas, W. D. Bowman, E. F. Zalewski and R. A. Velapoldi, *J. Phys. Chem.*, 1981, **85**, 2766-2771.
5. M. J. Frisch, G. W. Trucks, H. B. Schlegel, G. E. Scuseria, M. A. Robb, J. R. Cheeseman, G. Scalmani, V. Barone, G. A. Petersson, H. Nakatsuji, X. Li, M. Caricato, A. V. Marenich, J. Bloino, B. G. Janesko, R. Gomperts, B. Mennucci, H. P. Hratchian, J. V. Ortiz, A. F. Izmaylov, J. L. Sonnenberg, Williams, F. Ding, F. Lipparini, F. Egidi, J. Goings, B. Peng, A. Petrone, T. Henderson, D. Ranasinghe, V. G. Zakrzewski, J. Gao, N. Rega, G. Zheng, W. Liang, M. Hada, M. Ehara, K. Toyota, R. Fukuda, J. Hasegawa, M. Ishida, T. Nakajima, Y. Honda, O. Kitao, H. Nakai, T. Vreven, K. Throssell, J. A. Montgomery Jr., J. E. Peralta, F. Ogliaro, M. J. Bearpark, J. J. Heyd, E. N. Brothers, K. N. Kudin, V. N. Staroverov, T. A. Keith, R. Kobayashi, J. Normand, K. Raghavachari, A. P. Rendell, J. C. Burant, S. S. Iyengar, J. Tomasi, M. Cossi, J. M. Millam, M. Klene, C. Adamo, R. Cammi, J. W. Ochterski, R. L. Martin, K. Morokuma, O. Farkas, J. B. Foresman and D. J. Fox, *Gaussian 09*, 2013.
6. (a) A. D. Becke, *Phys. Rev. A*, 1988, **38**, 3098-3100; (b) C. T. Lee, W. T. Yang and R. G. Parr, *Phys. Rev. B*, 1988, **37**, 785-789.
7. (a) R. Krishnan, J. S. Binkley, R. Seeger and J. A. Pople, *J. Chem. Phys.*, 1980, **72**, 650-654; (b) A. D. McLean and G. S. Chandler, *J. Chem. Phys.*, 1980, **72**, 5639-5648; (c) M. M. Francl, W. J. Pietro, W. J. Hehre, J. S. Binkley, M. S. Gordon, D. J. Defrees and J. A. Pople, *J. Chem. Phys.*, 1982, **77**, 3654-3665.
8. (a) P. J. Hay and W. R. Wadt, *J. Chem. Phys.*, 1985, **82**, 299-310; (b) A. W. Ehlers, M. Bohme, S. Dapprich, A. Gobbi, A. Hollwarth, V. Jonas, K. F. Kohler, R. Stegmann, A. Veldkamp and G. Frenking, *Chem. Phys. Lett.*, 1993, **208**, 111-114; (c) L. E. Roy, P. J. Hay and R. L. Martin, *J. Chem. Theory Comput.*, 2008, **4**, 1029-1031.
9. B. P. Pritchard, D. Altarawy, B. Didier, T. D. Gibson and T. L. Windus, *J. Chem Inf. Model.*, 2019, **59**, 4814-4820.
10. V. Barone and M. Cossi, *J. Phys. Chem. A*, 1998, **102**, 1995-2001.
11. A. L. Tenderholt, *QMForge 2.4*, 2018.
12. F. Neese, *Wiley Interdiscip. Rev. Comput. Mol. Sci.*, 2018, **8**, 6.
13. F. Weigend and R. Ahlrichs, *Phys. Chem. Chem. Phys.*, 2005, **7**, 3297-3305.
14. (a) D. A. Pantazis, X.-Y. Chen, C. R. Landis and F. Neese, *J. Chem. Theory Comput.*, 2008, **4**, 908-919; (b) J. D. N. F. Rolfes, *J. Comput. Chem.*, 2020, **41**, 1842-1849.
15. J. P. Perdew, *Phys. Rev. B*, 1986, **33**, 8822-8824.
16. T. Yanai, D. P. Tew and N. C. Handy, *Chem. Phys. Lett.*, 2004, **393**, 51-57.
17. (a) A. E. Stiegman, V. M. Miskowski and H. B. Gray, *J. Am. Chem. Soc.*, 1986, **108**, 2781-2782; (b) A. E. Stiegman and V. M. Miskowski, *J. Am. Chem. Soc.*, 1988, **110**, 4053-4054; (c) P. M. Bradley, B. E. Bursten and C. Turro, *Inorg. Chem.*, 2001, **40**, 1376-1379; (d) M. A. Bennett, S. K. Bhargava, E. C.-C. Cheng, W. H. Lam, T. K.-M. Lee, S. H. Priver, J. Wagler, A. C. Willis and V. W.-W. Yam, *J. Am. Chem. Soc.*, 2010, **132**, 7094-7103.